Int. J. Metrol. Qual. Eng. **4**, 81–86 (2013)

DOI: 10.1051/ijmqe/2013040

# Determination of multilayer thicknesses of GaAs/AlAs superlattice by grazing incidence X-ray reflectivity

L.L. Ren*, H.F. Gao, S.T. Gao, J.J. Liu, and W. Zhang

National Institute of Metrology of China, Beijing 100013, P.R. China

Received: 19 November 2012 / Accepted: 11 July 2013

**Abstract.** The grazing incidence X-ray reflectivity is used to determine the multilayer thickness of GaAs/AlAs supperlattice. The measurement process includes the fitting model and the measurement conditions (different powers of 45 kV × 40 mA, 40 kV × 40 mA and 35 kV × 40 mA, different step sizes of 0.005°, 0.008° and 0.010°, and different times per step of 1 s, 2 s, 3 s). In order to obtain the valid measurement process, the combined standard deviation is used as the normal of the fitting results selection. As a result, the measurement condition of 0.008° step size and 2 s time per step with the power 40 kV × 40 mA is selectable with the operation stability of facilities and smaller error.

**Keywords:** Multilayer thickness; grazing incidence X-ray reflectivity; GaAs/AlAs supperlattice; combined standard deviation; valid measurement process

## 1 Introduction

Thin and multilayer films with thickness of a few nanometer are widely used in the solid state electronic and optoelectronic devices [1, 2]. Many techniques are used to characterize the thin film thickness. Sputter techniques like secondary ion mass spectrometry (SIMS) and sputter-assisted Auger electron spectroscopy (AES) allow the layer thickness and composition to be estimated, but they provide an absolute thickness only with reference to a standard. Optical methods like photoluminescence (PL) and atomic force microscopy (AFM) [3] give further information, but they impose restrictions on the structure to be investigated. Finally, transmission electron microscopy (TEM) allows the determination of the layer thickness; however, sample preparation is complicated and destructive [4]. Grazing incidence X-ray reflectivity (GIXRR) is a powerful and effective method for characterizing film thickness, surface/interface roughness and density for ultra layers without any damage of the materials [5–7]. Moreover, GIXRR is an absolute method to give the structure parameters without any reference to the standard. We have studied the traceability of the angle and wavelength of the GIXRR instrument in our institute [8, 9]. Single layers and multilayer stacks can be investigated without limits on the type of materials present [10–13].

However, the thickness obtained from GIXRR is based on the fitting results, which should compare the fitting curve with the measured curve. In fact, the fitting values are different even for fitting the same curve with satisfactory fitting plots if we slightly change the fitting parameters. As a result, the selection normal is needed to make sure the fitting results are reliable and measurement conditions are matched. As we know, reliable thickness results are critically important especially for thin films with thickness of a few nanometers, because even a 1 nm error will lead to device damage [14]. Previous research have been done on thin film thickness measurements by GIXRR [15–17], but few reports have focused on the reasons for the choice of parameters used to determine the film thickness. In this paper, we will use the combined standard deviation (CSD) as the normal of the result selection to discuss the determination of fitting results and optimal measurement conditions. The superlattice GaAs/AlAs with perfect film structure was measured in this paper to evaluate the accuracy of the measurement thickness.

## 2 Mechanism

The GIXRR measurement process includes obtaining the measurement plot and fitting this plot to obtain the final result. Different fitting parameters will lead to similar fitting curves, since slight variations in the thickness, density and roughness have little effect. In order to achieve reliable results, the measurement reliable evolution formula is used as shown in the formulas (1)–(4) [18], where $x_i$ is the result of the $i$th simulation, $n$ is the simulation times, $r$ is the repeatability, $x_m$ and $x_n$ are the separated simulation results, $s_r$ is the standard deviation and $\bar{x}$ is the average of the simulation results. When the results are fitted to the formula (3), they are reliable. Based on these formulas, at least three satisfactory simulations are obtained for the same plot, and every simulation is treated as a separate test. As a result, the average of all of valid simulation results is the final result.

In order to determine the best measurement condition, multi-measurements are applied at the same measurement

* Correspondence: renll@nim.ac.cn

condition, and then every plot is multi-simulated reliably based on the formula (3). Finally, the film thickness $\bar{x}_n$ from the simulation results is calculated by the formula (5), and the combined standard deviation (CSD) $s$ is calculated via the formula (6). $m$ is the valid simulation times and $\bar{x}_m$ is the average of valid simulation results for the same measurement, and $n_m$ is measurement times. $s_m$ is then the standard deviation of valid simulations for the same measurement with multi reliable simulations.

$$\bar{x} = \frac{\sum_1^n x_i}{\sum_1^n i} \tag{1}$$

$$s_r = \sqrt{\frac{\sum_1^n (x_i - \bar{x})^2}{n(n-1)}} \tag{2}$$

$$|x_m - x_n|\,|x_1 - x_2| \leqslant r \tag{3}$$

$$r = 2.83 s_r \tag{4}$$

$$\bar{x}_n = \frac{\sum n_m \bar{x}_m}{\sum n_m} \tag{5}$$

$$s = \sqrt{\frac{(n_1-1)\,s_1^2 + (n_2-1)\,s_2^2 + \ldots + (n_m-1)\,s_m^2}{n_1-1+n_2-1+\ldots+n_m-1}}. \tag{6}$$

## 3 Experiments

The GaAs/AlAs superlattice was grown by molecular-beam epitaxy (MBE). A semi-insulting epiready (100) GaAs wafer was used as a substrate. After oxide desorption of a substrate surface, a 500-nm-thick GaAs buffer layer was grown at 600° to minify the interface roughness as far as possible. Then the 3 periodic modulation of the fluxes of Ga/As and As/Al concentration was made and nearly stoichiometric GaAs/AsAl layers were obtained. By setting an identical time length for opening and closing of the fluxes of Ga/As and As/Al, the thickness of individual layers of nominal value 10 nm was obtained, except the first layer which was 20 nm.

Grazing incidence X-ray reflectivity measurements (GIXRR) were performed using a normal X-ray diffractometer PANalytical's X'Pert PRO system equipped with a parabolic multilayer X-ray mirror after collimation adjustment. The X-ray wavelength of Cu K$\alpha$ ($\lambda$ = 1.54178 Å) line was used for the measurements. The specular reflectivity curves were recorded with $\omega$–$2\theta$ scans. It employed the optical matrix method, based on the expressions of Parratt [18], for the simulation of GIXRR curves of layered systems by the version 1.2 of X'Pert reflectivity software.

The superlattice structures were characterized by cross-sectional analysis on a JEM-2010 electron microscope (JEOL Ltd., Japan).

## 4 Results and discussion

The GaAs/AlAs superlattice grown by molecular-beam epitaxy (MBE) was measured by TEM (shown in Fig. 1).

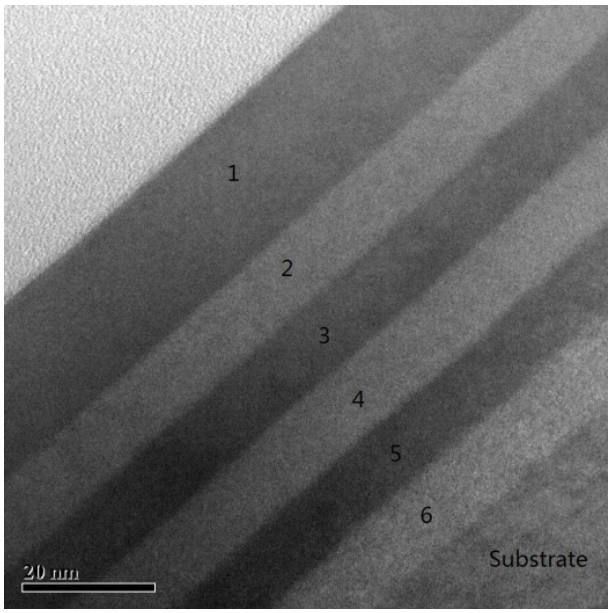


**Fig. 1.** The TEM image of the GaAs/AlAs.

**Table 1.** The thickness results by GIXRR and TEM.

| GaAs/AlAs film | GIXRR | TEM[a] |
|---|---|---|
| Oxide layer $\bar{x}_m$ | 0.99 | / |
| 1st $\bar{x}_m$ (nm) | 20.12 | 19.53 |
| 2st $\bar{x}_m$ (nm) | 10.60 | 10.34 |
| 3st $\bar{x}_m$ (nm) | 10.07 | 10.39 |
| 4st $\bar{x}_m$ (nm) | 10.59 | 10.76 |
| 5st $\bar{x}_m$ (nm) | 10.06 | 9.81 |
| 6st $\bar{x}_m$ (nm) | 10.59 | 10.33 |

[a] The average values of different position measurements.

**Table 2.** The fitting model of measured data.

| | |
|---|---|
| GaAs oxides (1 nm–5 nm) | |
| GaAs (20 nm) | |
| AlAs (10 nm)<br>GaAs (10 nm) | 3 periods |
| GaAs (substrate 350 000 nm) | |

The image shows that the superlattice is assembled layer by layer, indicating that we have obtained a well structured GaAs/AlAs superlattice. The thickness of every layer is assessed from the TEM image as shown in Table 1, which is consistent with the nominal value of layer thickness by MBE.

## 5 Fitting process

The previous research has shown that the fitting model has great effect on the simulation results [1]. Therefore, it's necessary to construct the fitting model based on the materials. In our research, GaAs and AlAs are very easy to be oxidation, so the fitting model is shown in Table 2.

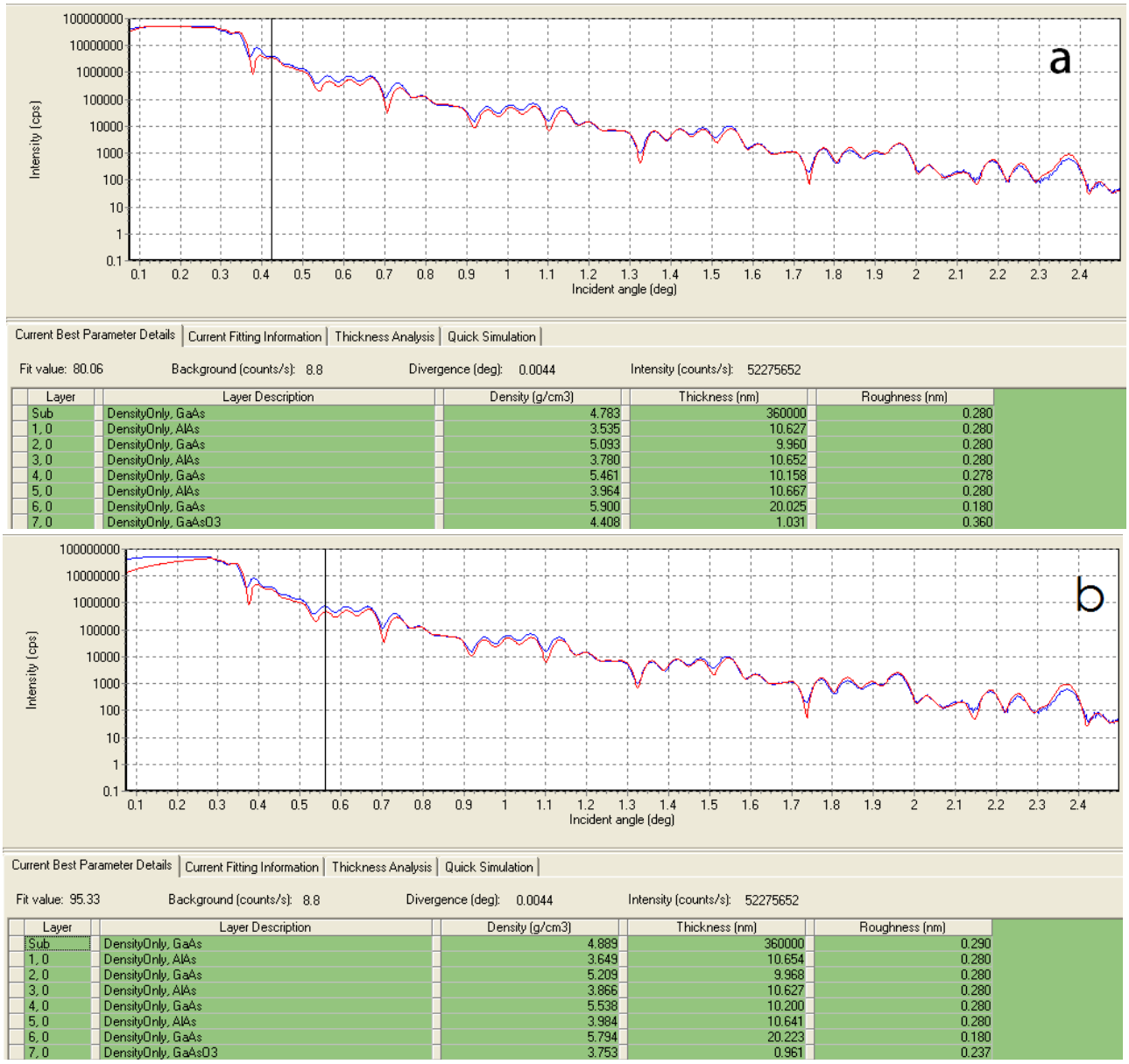


**Fig. 2.** The simulation results of superlattice determined by GIXRR.

There is an added oxide-layer in the fitting model, and the buffer layer is ignored due to its similar density with the substrate. The simulation results based on the fitting model in Table 1 are shown in Figure 2.

As shown in Figure 2, excellent agreements between experimental data and theoretical simulations are obtained with the different fitting parameters, indicating that our fitting model is right, but the simulation results between Figures 2a and 2b, such as density, roughness and thickness show some differences. So we need a certiorari to define the final results. Because the thin film thickness is of critical importance for applications, it is used to study the reliable simulations and measurement process.

Based on the formulas (1)–(4), at least three satisfactory simulations are obtained for the same plot, and every simulation is treated as a separate test. When the results are fitted to the formula (3), they are reliable. As a result, the average of all of the valid simulation results is the final result. The fitting results are shown in Table 1. The final thicknesses are consistent with the TEM results.

## 6 Measurement conditions

Figure 3 is the overlay of measurement plots of the GaAs/AlAs superlattice at the step size 0.008° and the time per step of 2.00 s and different powers, 45 kV × 40 mA, 40 kV × 40 mA and 35 kV × 40 mA, separately. As shown in Figure 3, the plots are a little different and we cannot indicate which condition is better. In order to determine the better measurement condition, four measurements are applied at every same measurement condition,

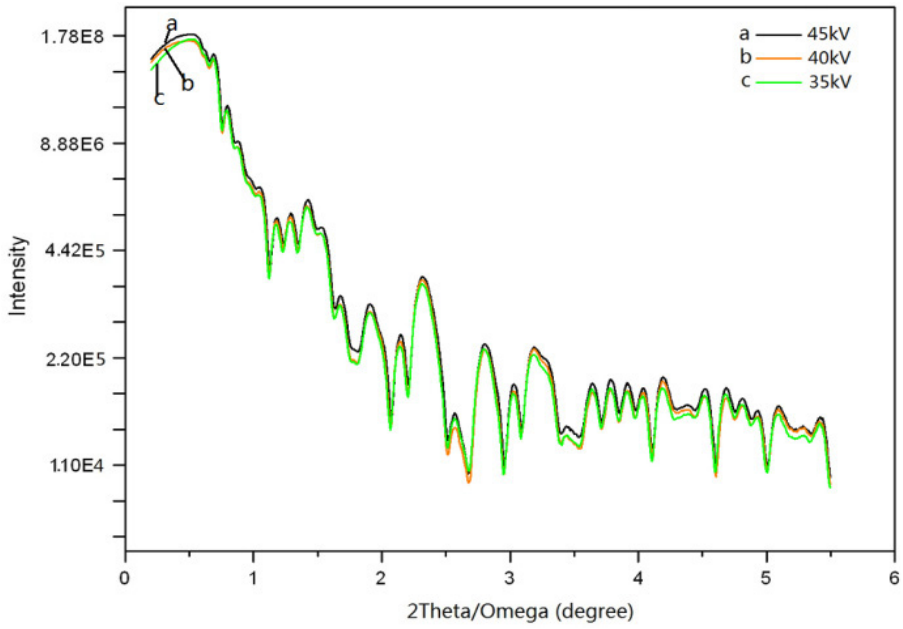


**Fig. 3.** Measurement plots of the GaAs/AlAs superlattice by XRR at powers (a) 45 kV × 40 mA, (b) 40 kV × 40 mA, (c) 35 kV × 40 mA.

and then every plot is multi-simulated based on the formula (3). Finally, the film thickness $\bar{x}_n$ from the simulation results is calculated by the formula (5), and the combined standard deviation (CSD) $s$ is calculated via the formula (6), which are shown in Figure 4.

As shown in Figure 4a, the thicknesses are consistent at the powers 45 kV × 40 mA and 40 kV × 40 mA, but the CSDs of simulation thicknesses at power 40 kV × 40 mA is smaller than those at powers 45 kV × 40 mA and 35 kV × 40 mA with big fluctuations. The reason is probably that the lower incident X-ray power of 35 kV × 40 mA causes more noise, so the determined thickness is not consistent with the others and the CSD is higher. When the power is 45 kV × 40 mA, which is near to the limited power of the facility, the incident X-ray energy is high, but the stability of the facility decreases, as a result, this thickness is reliable while its CSD is large. As we know, the CSD is smaller indicating that the measurement condition is better. So the CSD is a ruler for the confirmation of the results. Therefore, the power 40 kV × 40 mA is a good condition for GIXRR measurements.

In order to save operation time and keep the high measurement accuracy, different step sizes of 0.005°, 0.008° and 0.010° and different times per step of 1 s, 2 s, 3 s with the power of 40 kV × 40 mA were studied. Similarly, the thicknesses and CSDs are calculated based on the formulas (5) and (6) shown in Figure 5.

As shown in Figures 5a and 5b, the thicknesses are consistent and the CSDs are small at the lower step size 0.005° and 0.008°. The main reason is probably that more counts are collected and simulated at smaller step size. However, the measurement time is more prolonged at the 0.005° step size than at the 0.008° step size, so we suggest that the 0.008° step size is the better selection.

Figure 6 is the thicknesses and CSDs of simulation results at different time per step with the 0.008° step size

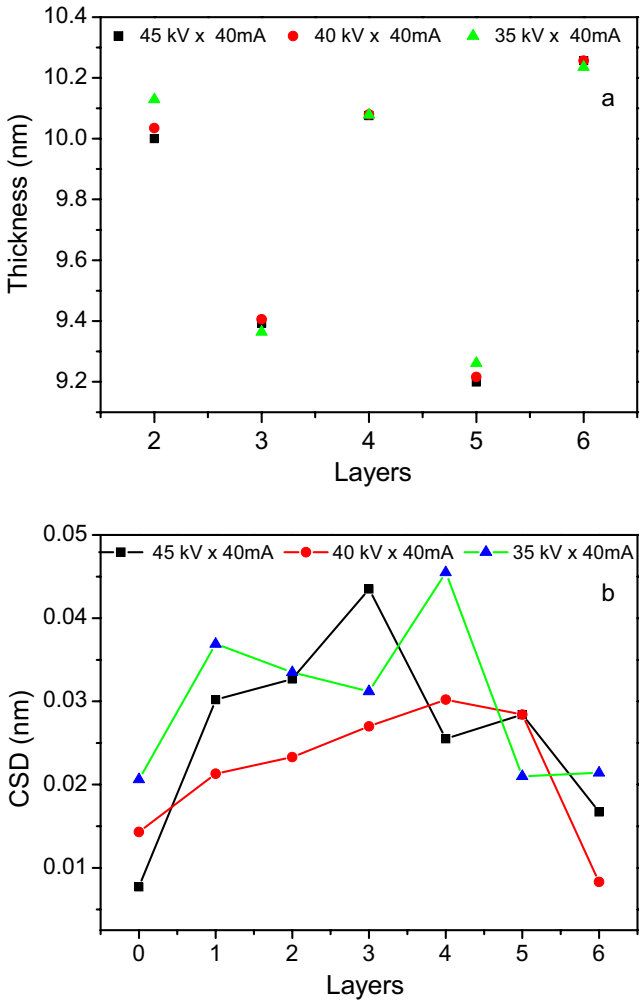


**Fig. 4.** The thicknesses (a) and MSDs (b) of simulation results at powers (■) 45 kV × 40 mA, (●) 40 kV × 40 mA, (▲) 35 kV × 40 mA.

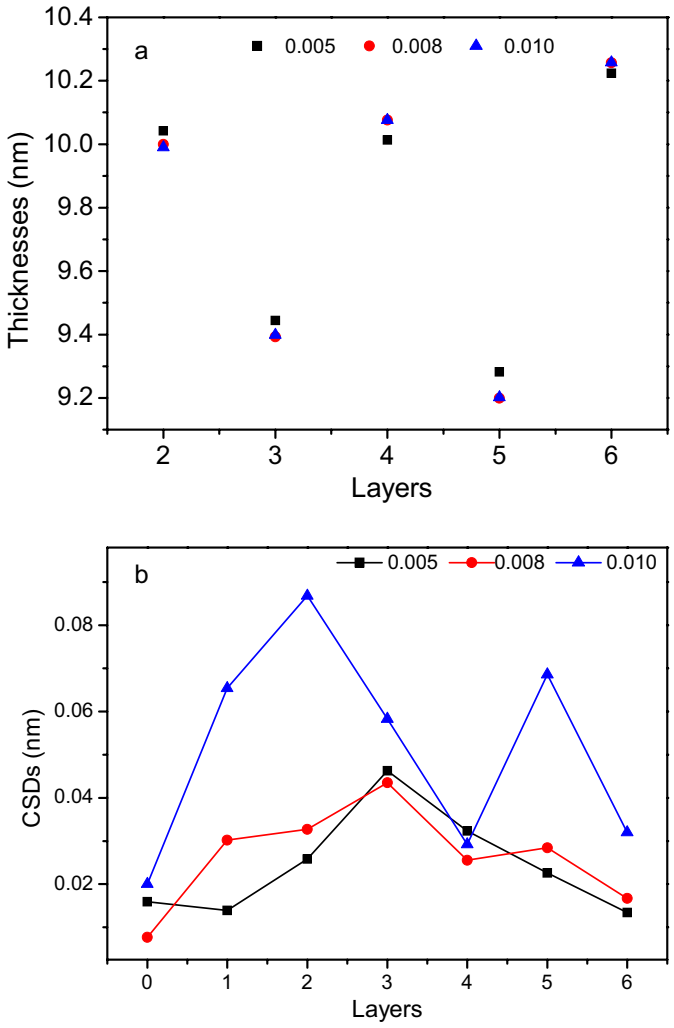


**Fig. 5.** The thicknesses (a) and MSDs (b) of simulation results at step size (■) 0.005°, (●) 0.008°, (▲) 0.010°.

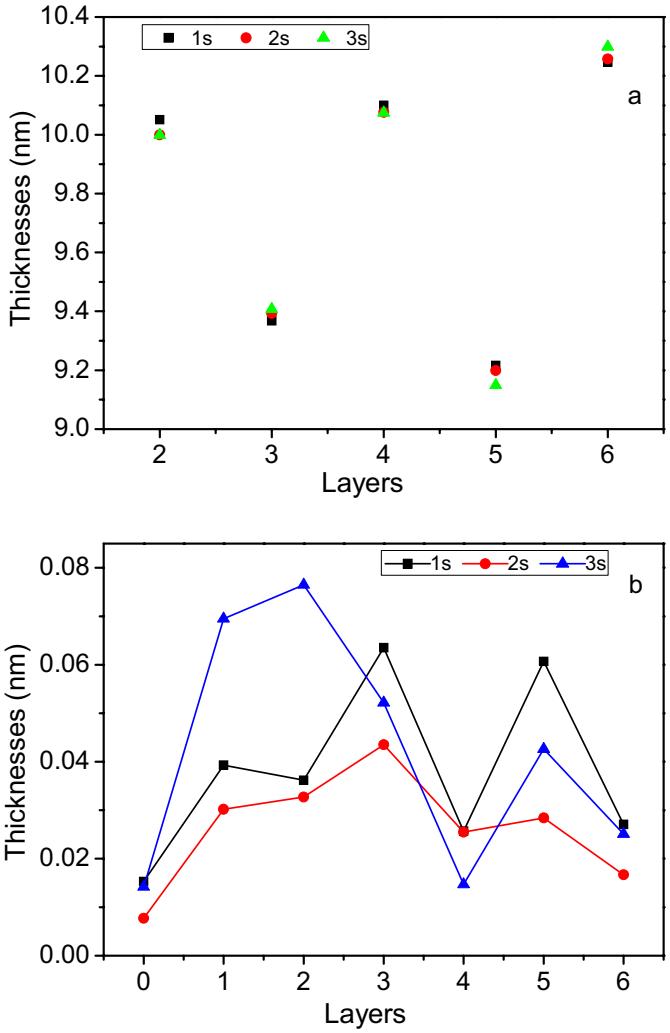


**Fig. 6.** The thicknesses (a) and MSDs (b) of simulation results at time per step (■) 1 s, (●) 2 s, (▲) 3 s.

and power of 40 kV × 40 mA. As shown in Figure 6a, the thicknesses are selectable when the time per step is 2 s. Moreover, the CSDs and their fluctuation at the time per step 2 s is the lowest in Figure 6b. Because the time per step decides the time of collection, more counts are collected at the longer time per step, such as 3 s, while fewer counts were collected at shorter time per step (1 s). However, more counts probably include more noise, so it would cause higher CSDs. So we suggest the time per step of 2 s is a good selection.

## 7 Conclusions

The measurement process of GIXRR technology includes the fitting process and the measurement conditions. The combined standard deviation is a valid ruler for the fitting result and measurement condition selections. For the operation stability of facilities and smaller error, the measurement condition of 0.008° step size and 2 s time per step with power 40 kV × 40 mA is preferable. The thickness results by GIXRR are consistent with those by TEM.

*Acknowledgements.* Dr. Toshiyuki Fujimoto gave useful discussions about the measurement process. This work was supported by AQSIQ and NIM with Grant Nos. AHY0913 and AKY1006.

## References

1. C.-S. Kim, T.-K. Koo, Y.-D. Choi, Observation of an Interlayer in a Nano-Scale $SiO_2$ Layer on Si Substrate by X-Ray Reflectivity (XRR) Analysis, Solid State Phenom. **124–126**, 1689–1692 (2007)
2. C. Schug, B. York, J. Marien, H.-R. Blank, JCPDS-International Center for Diffraction Data 2001, Adv. X-Ray Anal. **44**, 295–301 (2001)
3. G. Friedbacher, P.K. Hansma, D. Schwarzbach, M. Grasserbauer, H. Nickel, Investigation of aluminum gallium arsenide/gallium arsenide superlattices by atomic force microscopy, Anal. Chem. **64**, 1760–1762 (1992)

4. D.G. Rickerby, T. Friesen, Microstructural examination of layered coatings by scanning electron microscopy, transmission electron microscopy, and atomic force microscopy, Mater. Charact. **36**, 213–223 (1996)
5. D.K. Bowen, M. Wormington, Characterization of materials by grazing-incidence X-ray scattering, Adv. X-Ray Anal. **36**, 171 (1993)
6. K.N. Stoev, K. Sakurai, Review on grazing incidence X-ray spectrometry and reflectometry, Spectrochim. Acta Part B **54**, 41 (1999)
7. T.C. Chen, C.-Y. Peng, C.-H. Tseng, M.-H. Liao, M.-H. Chen, C.-I. Wu, M.-Y. Chern, P.-J. Tzeng, C.W. Liu, Characterization of the Ultrathin $H_fO_2$ and $H_f$-Silicate Films Grown by Atomic Layer Deposition, IEEE Trans. Electron Devices **54**, 759–766 (2007)
8. L. Ren, J. Cui, The Angle Traceablity of X-ray Diffraction, Metrol. Technol. **3**, 48–51 (2012)
9. L. Ren, H. Gao, The X-ray Wavelength Traceablity of X-ray Diffraction, Metrol. Technol. **12**, 3–4 (2012)
10. W. Xia, B.A. Minch, M.D. Carducci, N.R. Armstrong, LB films of rodlike phthalocyanine aggregates: Specular X-ray reflectivity studies of the effect of interface modification on coherence and microstructure, Langmuir **20**, 7998–8005 (2004)
11. F. Cecchet, B. De Meersman, S. Demoustier-Champagne, B. Nysten, A.M. Jonas, One step growth of protein antifouling surfaces: monolayers of poly (ethylene oxide)(PEO) derivatives on oxidized and hydrogen-passivated silicon surfaces, Langmuir **22**, 1173–1181 (2006)
12. S. Basu, S.K. Satija, In-situ X-ray Reflectivity Study of Alkane Films Grown from the Vapor Phase, Langmuir **23**, 8331–8335 (2007)
13. C.R. Hansen, T.J. Sørensen, M. Glyvradal, J. Larsen, S.H. Eisenhardt, T. Bjørnholm, M.M. Nielsen, R. Feidenhans'l, B.W. Laursen, Structure of the Buried Metal-Molecule Interface in Organic Thin Film Devices, Nano Lett. **9**, 1052–1057 (2009)
14. W.H. Briscoe, M. Chen, I.E. Dunlop, J. Klein, J. Penfold, R.M.J. Jacobs, Applying grazing incidence X-ray reflectometry (XRR) to characterising nanofilms on mica, J. Coll. Interf. Sci. **306**, 459–463 (2007)
15. O. Durand, V. Berger, R. Bisaro, A. Bouchier, A. De Rossi, X. Marcadet, I. Prevot, Determination of thicknesses and interface roughnesses of GaAs-based and InAs/AlSb-based heterostructures by X-ray reflectometry, Mater. Sci. Semicond. Process. **4**, 327–330 (2001)
16. A. Gibaud, S. Hazra, X-ray reflectivity and diffuse scattering, Curr. Sci. **78**, 1467–1477 (2000)
17. Rusli, K. Chew, S.F. Yoon, H.K. Chan, C.F. Ng, Q. Zhang, J. Ahn, Determination of Properties of Thin Films Using X-ray Reflectivity, Int. J. Mod. Phys. B **16**, 1072 (2002)
18. L.G. Parratt, Surface Studies of Solids by Total Reflection of X-Rays, Phys. Rev. **95**, 395–369 (1954)
19. H. Quan, Y.Z. Han, *Reference Materials and Their Applications*, 2nd edn. (Chinese Standard Press, Beijing, 2003)